

## Structure and stability of CN adlayers on Rh(110)

Federica Bondino<sup>a</sup>, Alessandro Baraldi<sup>b</sup>, Giovanni Comelli<sup>a</sup>, Falko P. Netzer<sup>c,\*</sup>

<sup>a</sup> TASC-INFM Laboratory, Padriciano 99, I-34012 Trieste, Italy and Dipartimento di Fisica, Università di Trieste, via Valerio 2, I-34127 Trieste, Italy

<sup>b</sup> Sincrotrone Trieste, S.S. 14 Km 163.5, 34012 Trieste, Italy

<sup>c</sup> Institut für Experimentalphysik, Karl-Franzens-Universität Graz, A-8010 Graz, Austria

Received 21 January 2000; accepted for publication 3 April 2000

### Abstract

The formation and stability of CN adlayers on Rh(110), formed by dissociative adsorption of  $C_2N_2$  at 373 K, have been studied as a function of coverage and temperature by low-energy electron diffraction (LEED), X-ray photoelectron spectroscopy (XPS), and thermal desorption spectroscopy (TDS). Two different CN adsorption states have been distinguished by their different C 1s and N 1s XPS core-level binding energies. The CN-I state is exclusively occupied up to a surface coverage of 0.5 monolayers (ML), where a well-ordered  $c(2 \times 2)$  LEED pattern is observed. The CN-II state becomes additionally populated at higher coverages from 0.5 ML to the saturation coverage of 0.87 ML. At CN saturation, a  $c(4 \times 2)$  LEED structure is formed. Desorption of CN as molecular  $C_2N_2$  occurs only for surface coverages  $>0.5$  ML and appears to be mainly derived from the CN-II state. The onset of C–N bond rupture is indicated at  $\sim 450$ – $550$  K, depending on the CN coverage; the resulting  $N_{ad}$  desorbs at  $\sim 580$  K from the more crowded surface and in the range of  $\sim 650$ – $950$  K, whereas  $C_{ad}$  remains at the Rh surface and cannot be desorbed thermally. © 2000 Elsevier Science B.V. All rights reserved.

**Keywords:** Cyanogen; Low energy electron diffraction (LEED); Rhodium; X-ray photoelectron spectroscopy

### 1. Introduction

Rhodium is an important metallic constituent in catalytic automotive converters. One of the reasons for using the expensive Rh in the three-way catalysts of automotive exhausts is that it appears to be particularly active for the removal of NO, via the  $NO + CO$  reaction, converting it to  $N_2$  and  $CO_2$ , or by reduction with hydrocarbons. The formation of cyanide intermediates in the catalytic reduction of NO by  $C_2H_4$  on Rh(111) surfaces [1,2] and during the interaction of CO and NO on ceria supported Rh surfaces [3]

has been reported recently. The knowledge of the adsorption properties of CN species on Rh surfaces is therefore an important prerequisite to assess the surface chemistry of these cyanide reaction intermediates. Moreover, interest in CN surface chemistry on Rh derives from many large-scale industrial processes, such as the Andrussov process for the synthesis of HCN from  $CH_4$ ,  $NH_3$ , and  $O_2$  over Rh–Pt surfaces. The bonding and surface stability of CN species also have a model character for the surface interactions of organic and polymeric nitriles [4], where the CN functional groups provide important centres for surface attachment.

The adsorption and decomposition of  $C_2N_2$  to form CN on Rh(111) has been studied by Solymosi and Bugyi [5] and Hwang et al. [6] using

\* Corresponding author. Fax: +43-316-3809816.  
E-mail address: netzer@kfunigraz.ac.at (F.P. Netzer)

Auger electron spectroscopy, LEED, and thermal desorption spectroscopy (TDS). Both studies agree that above room temperature, adsorbed  $C_2N_2$  dissociates to form surface CN, which in turn partly dissociates at a higher temperature into  $N_{ad}$  and  $C_{ad}$ , but partly also desorbs as  $C_2N_2$  for higher CN coverages. Below room temperature, molecular  $C_2N_2$  adsorption has been inferred indirectly [5,6]. No ordered LEED pattern has been observed for CN on Rh(111) [5].

Here, we report a study of the structure and surface stability of CN adlayers on Rh(110), using LEED, X-ray photoelectron spectroscopy (XPS), and TDS. The CN surface species have been obtained by dissociative adsorption of  $C_2N_2$  at 373 K. We have investigated the formation of the CN adlayers as a function of coverage and have observed the formation of several ordered CN surface structures in LEED. The absolute CN coverages have been determined by C 1s and N 1s core-level XPS, using a well-ordered  $c(2 \times 2)$  LEED structure as the calibration point. The competitive processes of C–N bond cleavage and associative  $C_2N_2$  desorption have been specified as a function of temperature and coverage. Moreover, plausible models of the ordered CN LEED structures and a consistent description of their evolution with increasing surface population are presented.

## 2. Experimental

The experiments were carried out in a standard UHV chamber equipped with a rear-view LEED, a 150 mm mean radius hemispherical electron energy analyser with a multichannel detector, a conventional laboratory X-ray source, a quadrupole mass spectrometer and facilities for gas inlet and sample cleaning. The XPS spectra were taken using the  $MgK\alpha$  source operated at 800 W power and with a fixed analyser pass energy of 20 eV. The binding energies were calibrated using the Rh  $3p_{3/2}$  peak as a reference. Thermal desorption experiments were performed with the sample in front of the mass spectrometer using a linear temperature ramp of 3 K/s. The chamber is also equipped with an Omicron SPA-LEED system, which allows diffraction spot profiles to be mea-

sured. The use of a channeltron, mounted behind a 100  $\mu m$  aperture, makes it possible to use an electron beam current of less than 0.1  $\mu A$ , thus minimizing damage to the adsorbate layer under investigation. The transfer width of the instrument is better than 1000  $\text{\AA}$  at an electron kinetic energy of 85 eV.

The sample, a Rh(110) disk, was mounted on to the manipulator through two tungsten wires and heated by direct current. The cleaning procedure involved repeated cycles of  $Ar^+$  bombardment at room temperature and annealing to 1300 K followed by oxygen treatment at 1100 K (10 min,  $1 \times 10^{-7}$  mbar). The sample was then flashed to 1300 K and, while cooling, reduced in hydrogen ( $5 \times 10^{-7}$  mbar) in order to remove any residual oxygen. Cyanogen was produced by thermal decomposition of AgCN in a tube attached to the gas line.

## 3. Results

Fig. 1 illustrates the formation of a CN adlayer on Rh(110) after exposure to 20 L  $C_2N_2$  [1 Langmuir (L) =  $1 \times 10^{-6}$  Torr.s] at 100 K followed by stepwise annealing to 375 K. Fig. 1a displays a sequence of N 1s core-level spectra, whereas Fig. 1b shows the corresponding C 1s XPS spectra. After adsorption at 100 K, two spectral structures are observed at  $397.8 \pm 0.1$  and 399.5 eV for the N 1s and at  $284.7 \pm 0.1$  and 287 eV for the C 1s spectra. The peaks at the higher binding energies (BE) (399.5 and 287 eV for N 1s and C 1s, respectively) are similar to the  $C_2N_2$  multilayer structures observed on Pd(110) [7] and are therefore also associated here with a condensed  $C_2N_2$  phase. The structures at 397.8 eV (N 1s) and 284.7 eV (C 1s) then derive from the molecular  $C_2N_2$  monolayer. On heating, the condensed  $C_2N_2$  desorbs, and at  $\sim 200$  K, the monolayer is left at the surface. Note that no ordered LEED pattern has been observed from the  $C_2N_2$  monolayer on Rh(110), in contrast to the  $c(2 \times 2)$  LEED patterns observed on Pd(110) [8] and Ni(110) surfaces [9]. Further annealing induces dissociation of  $C_2N_2$  to adsorbed CN, which is characterized by C 1s and N 1s binding energies

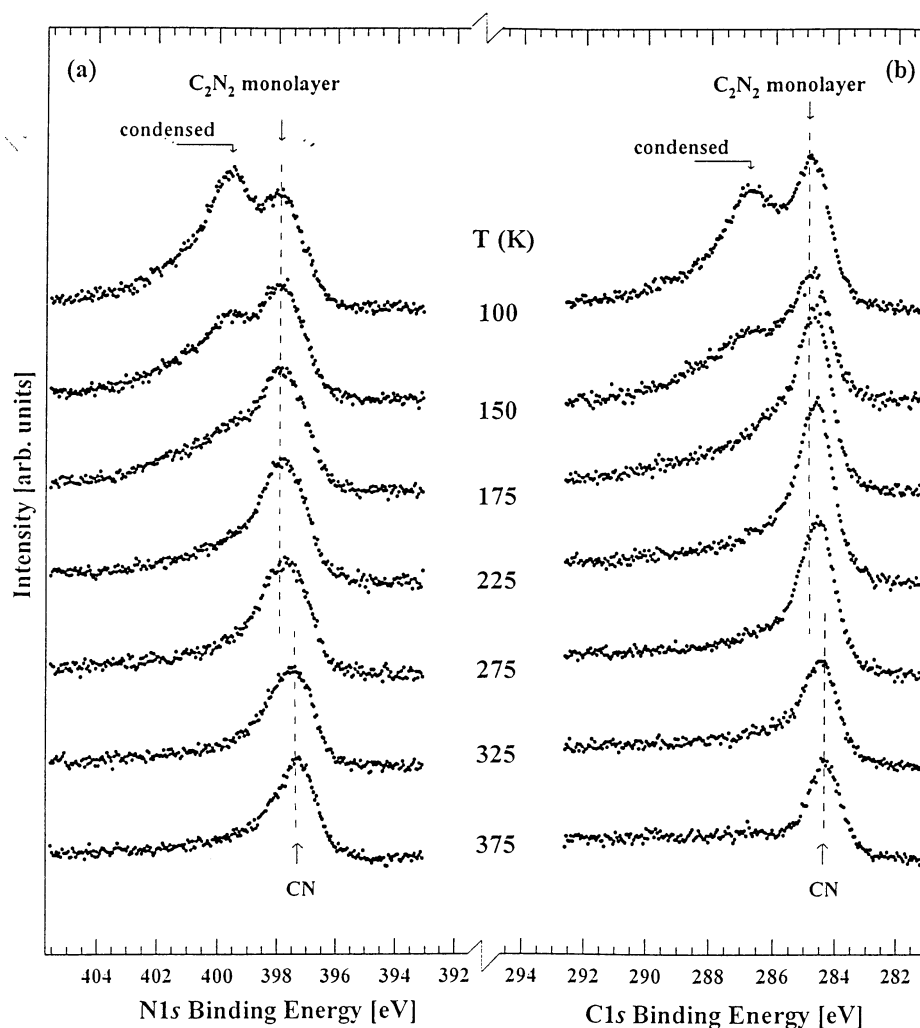


Fig. 1. N 1s (a) and C 1s (b) XPS core-level spectra of the Rh(110) surface exposed to 20 L  $C_2N_2$  at 100 K and heated subsequently to the indicated temperatures. The assignment of XPS peaks to various surface species is indicated.

of 284.3 and 397.4 eV, respectively. At room temperature ( $\sim 300$  K), the dissociation of  $C_2N_2$  into CN appears to be still somewhat incomplete, as also suggested by the TDS reported in the literature, where a so-called  $\alpha$   $C_2N_2$  desorption peak between 310 K [5] and 380 K [6] has been associated with desorption from a molecular  $C_2N_2$  adsorption state. The XPS spectra of Fig. 1 recorded after annealing to 373 K indicate, however, that at that temperature, all  $C_2N_2$  has dissociated into  $CN_{ad}$ . Since the prime interest of this study focuses on the adsorption of CN, the

following  $C_2N_2$  dosing experiments have all been carried out at 373 K, to ensure the formation of pure CN adlayers.

In Fig. 2, N 1s and C 1s XPS spectra are presented for increasing CN surface coverages on Rh(110). The areas under the nitrogen XPS peaks have been taken to derive the absolute CN surface coverage, using the sharp  $c(2 \times 2)$  LEED pattern observed (see below) for calibration purposes, with a coverage of 0.5 ML. The corresponding coverages are indicated in Fig. 2, together with the two major LEED structures observed. Up to a coverage

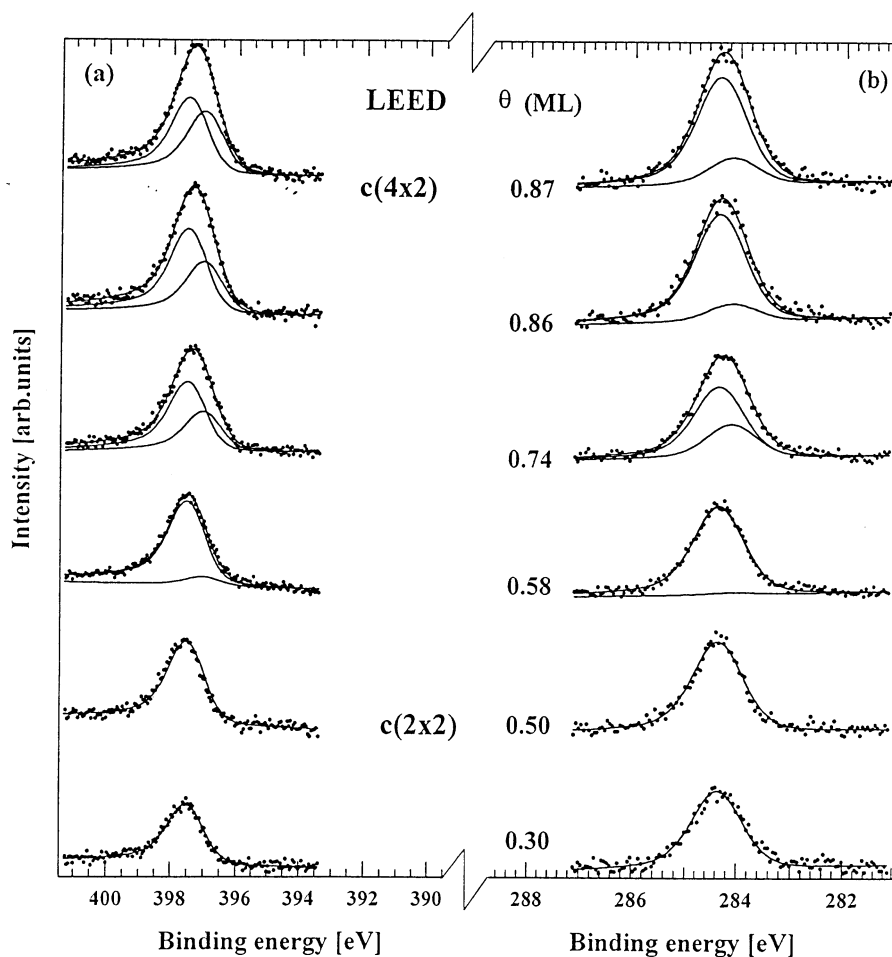


Fig. 2. N 1s (a) and C 1s (b) XPS core-level spectra of CN on Rh(110) as a function of CN surface coverage.

of 0.5 ML, the XPS data can be fitted with a single peak. For the analysis, the spectral profiles have been represented by Doniac–Sunjic line shapes (Lorentzian width  $\Gamma_L = 0.30$  eV for C 1s and 0.32 eV for N 1s) convoluted by a Gaussian (Gaussian width = 0.95 eV, i.e., fixed to the experimental resolution). The parameters obtained for fitting at low coverages have then been applied to the whole set of data. Thus, the  $c(2 \times 2)$  LEED structure contains a single CN adsorption state, henceforth designated as CN-I, with N 1s and C 1s binding energies of  $397.4 \pm 0.1$  and  $284.3 \pm 0.1$  eV, respectively. Above 0.5 ML CN coverage, it was not possible to fit the N 1s and C 1s data with a single peak with fixed BE. Thus, we added second

components to the analysis of the higher coverage spectra, located at  $397.0 \pm 0.1$  eV and  $284.1 \pm 0.1$  eV for N 1s and C 1s, respectively (CN-II). The N 1s and C 1s XPS binding energies of all CN-derived surface species observed on Rh(110) are collected in Table 1.

Fig. 3 shows an uptake curve of CN on Rh(110) in form of a plot of the CN coverage versus  $C_2N_2$  exposure at 373 K. The figure contains the total CN coverage and the coverage curves of the CN-I and CN-II adsorption states as derived from the two components of the curve-fitting analysis of the N 1s spectra. The delayed population of the CN-II state is clearly apparent from Fig. 3. The plots obtained from the C 1s peaks (not shown)

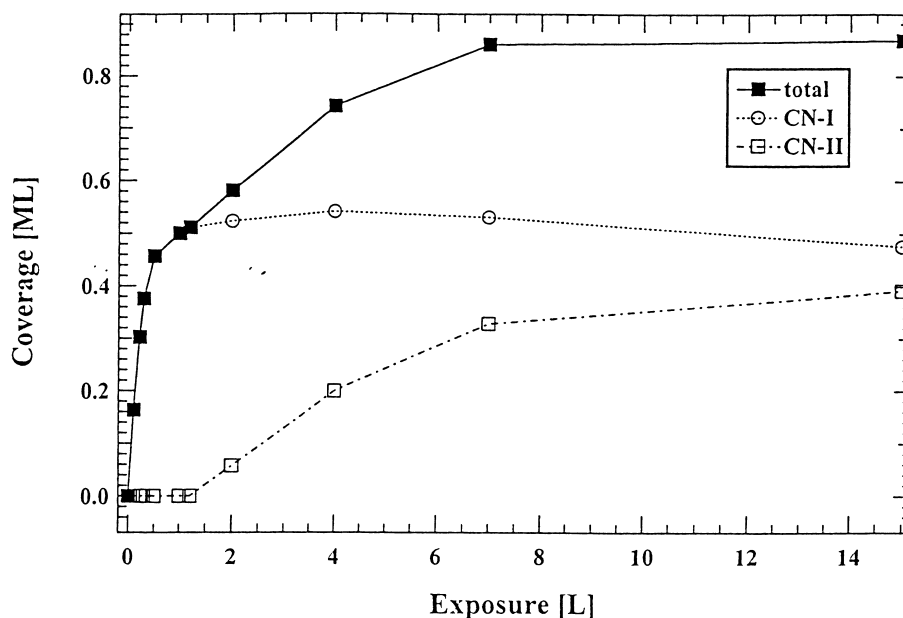


Fig. 3. CN uptake curve on Rh(110), in form of a plot of the CN coverage versus  $C_2N_2$  exposure at 373 K. The total CN coverage and the coverage curves of the CN-I and CN-II adsorption states are given.

follow a similar behaviour, but the coverage ratio between the CN-I and CN-II species is different. We believe that the information obtained from the N 1s area is more reliable, for the following reasons: (1) the CN-I and CN-II components are better separated in the N 1s region; (2) the cross-section of the N 1s electrons is higher, yielding better statistics; (3) in case the CN species are tilted with the C end down, as found for CN on Ni(110) [12], photoelectron diffraction effects are expected to be more relevant for the C 1s peak.

Fig. 4 shows the evolution of LEED patterns with increasing CN surface coverage, obtained after  $C_2N_2$  dosing on to Rh(110) at 373 K. After

$\sim 0.2$  L  $C_2N_2$  exposure, weak diffuse  $(1/2 \ 1/2)$  order reflexes first develop, which are elongated along the [01] direction (Fig. 4a). These reflexes then evolve into two distinct spots, thus forming a  $c(2 \times 2)$  structure with split spots along [01]. The spots move closer together with increasing exposure (0.4–1 L), until a sharp  $c(2 \times 2)$  pattern is observed best after  $C_2N_2$  exposure of 1 L (Fig. 4b). The spot profiles as a function of exposure have been measured quantitatively using the SPA-LEED apparatus (not shown), and the fully developed  $c(2 \times 2)$  structure has been used for coverage calibration purposes, as described above. For  $C_2N_2$  doses between 1 and 8 L, the  $(1/2 \ 1/2)$  order reflexes become split again, but this time along the [10] direction (Fig. 4c). The separation of the reflexes increases continuously up to the maximum coverage of 0.87 ML, where a well-ordered  $c(4 \times 2)$  pattern is observed (Fig. 4d). On annealing the sample to  $> 375$  K, this sequence of structures can be observed in reverse order. The  $c(2 \times 2)$  pattern vanishes completely at  $\sim 823$  K.

The temperature evolution and thermal stability of the CN adlayers have been followed by TDS and XPS. Let us consider first the TDS results in

Table 1  
C 1s and N 1s core-level binding energies of  $C_2N_2$ - and CN-derived surface species on Rh(110)

	N 1s (eV)	C 1s (eV)
$C_2N_2$ multilayers	399.5	287.0
$C_2N_2$ monolayer	397.8	284.7
CN-I	397.4	284.3
CN-II	397.0	284.1
$N_{ad}$ , $C_{ad}$	397.9	283.8

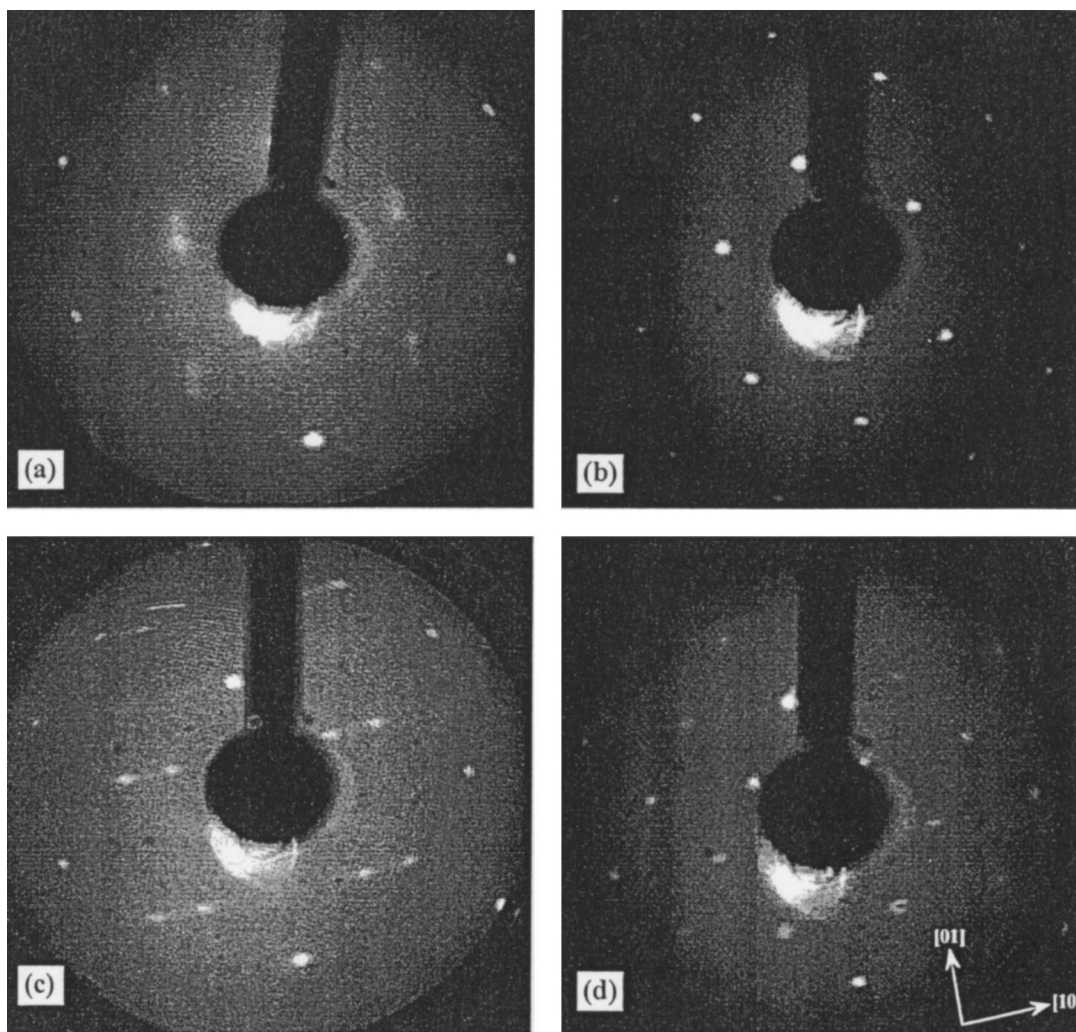


Fig. 4. LEED patterns of CN on Rh(110). (a)  $c(2 \times 2)$  pattern with split spots along the [01] surface direction (corresponding to the [001] crystal direction). (b)  $c(2 \times 2)$  pattern. (c)  $c(2 \times 2)$  pattern with split spots along the [10] surface direction (corresponding to the  $[1\bar{1}0]$  crystal direction). (d)  $c(4 \times 2)$  pattern.

Fig. 5. Fig. 5 contains TDS spectra of atomic mass units 12, 52, 14, and 28 (from bottom to top), corresponding to  $C_2N_2$  (52, 12) and  $N_2$  (28, 14); the desorption of undesired CO minority species, picked up by the surface from the system ambient or from the  $C_2N_2$  source, can be identified by cross-examination of the AMU 14 and 28 spectra. Molecular  $C_2N_2$  desorption is observed only for CN surface coverages  $> 0.5$  ML in a single desorption peak between 473 and 623 K, with the peak maximum shifting from 583 K initially to 543 K

at saturation coverage (see AMU 12 and 52 spectra). Note that no  $C_2N_2$  desorption occurs from the  $c(2 \times 2)$  CN overlayer.

The AMU 28 spectra show a more complicated behaviour, with several overlapping desorption peaks. We distinguish a weak feature at around 500 K for low coverages, a structure at 570 K for high coverages, and a broad two-peaked desorption feature in the range of 700–950 K. The lower-temperature peak of this latter structure is initially located at  $\sim 660$  K and shifts to 770 K at higher

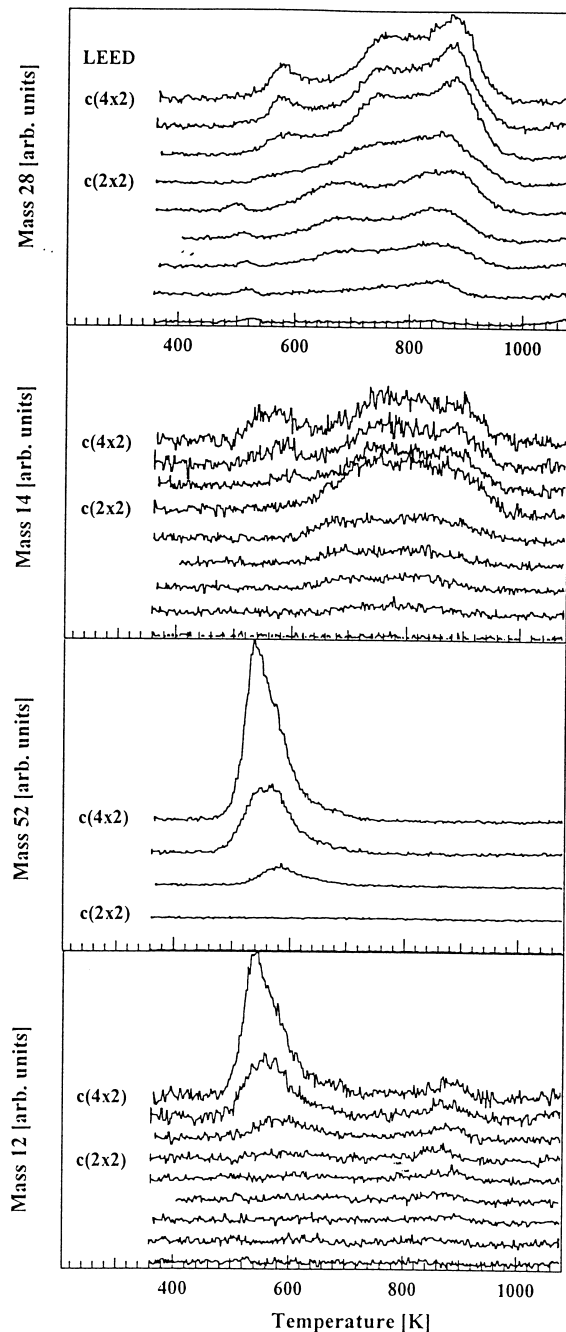


Fig. 5. Thermal desorption spectra of CN on Rh(110) displaying desorption curves of atomic mass units 12, 52, 14, and 28. The surface coverages increase from bottom to top curves in each panel. The corresponding LEED patterns are indicated. Heating rate 3 K/s.

coverages. The second peak maximum is seen at around 860–880 K. The signal of AMU 28 can in principle be related to  $N_2$  and CO molecules.  $N_2$  desorption is expected from the recombination of adsorbed N atoms generated by the C–N bond cleavage process. The AMU 14 spectra allow desorbing  $N_2$  to be distinguished from CO. The AMU 14 spectra show a good correspondence with the AMU 28 spectra apart from the small AMU 28 feature at  $\sim 500$  K at low coverages, which is thus revealed as due to minor CO desorption.  $N_2$  desorption is therefore identified at 570 K for high CN coverages and in the broad range of 660–950 K.

The thermal behaviour of CN adlayers on Rh(110) in XPS is illustrated in Fig. 6. Fig. 6a contains a sequence of N 1s spectra, and Fig. 6b a set of C 1s spectra, as a function of annealing to the indicated temperatures of the initially CN saturated surface ( $\theta_{CN} = 0.87$  ML). At higher temperatures ( $> 500$  K), the XPS data could not be fitted with the same parameters as those used for the spectra after adsorption at 373 K: third spectral components had to be introduced in the analysis, with a N 1s BE of 397.9 eV and a C 1s BE of 283.8 eV. These components are associated with atomic  $N_{ad}$  and  $C_{ad}$ , formed by the CN decomposition via C–N bond scission. Their binding energies are included in Table 1.

A detailed analysis of the XPS core-level spectra of Fig. 6 in terms of the (de)population of different CN derived surface species as a function of temperature is given in Fig. 7a, for N 1s and Fig. 7b for C 1s. Fig. 7a demonstrates that the total N 1s signal decreases gradually from  $\sim 450$  K on and vanishes at  $\sim 900$  K. In contrast, the total C 1s signal intensity (Fig. 7b) is still about a half of its initial value at that temperature. Both N 1s and C 1s signals show that the CN-II state becomes depopulated first, disappearing from the surface at 550–600 K. In conjunction with the TDS results of Fig. 5, this indicates that the disappearance of the CN-II species is correlated with the desorption of  $C_2N_2$ . The CN-I-related N 1s and C 1s signals remain approximately constant up to  $\sim 550$ –600 K and then decrease gradually. Concomitantly, the atomic adsorbate signals of  $N_{ad}$  and  $C_{ad}$  appear. This signals the dissociation of the CN-I species

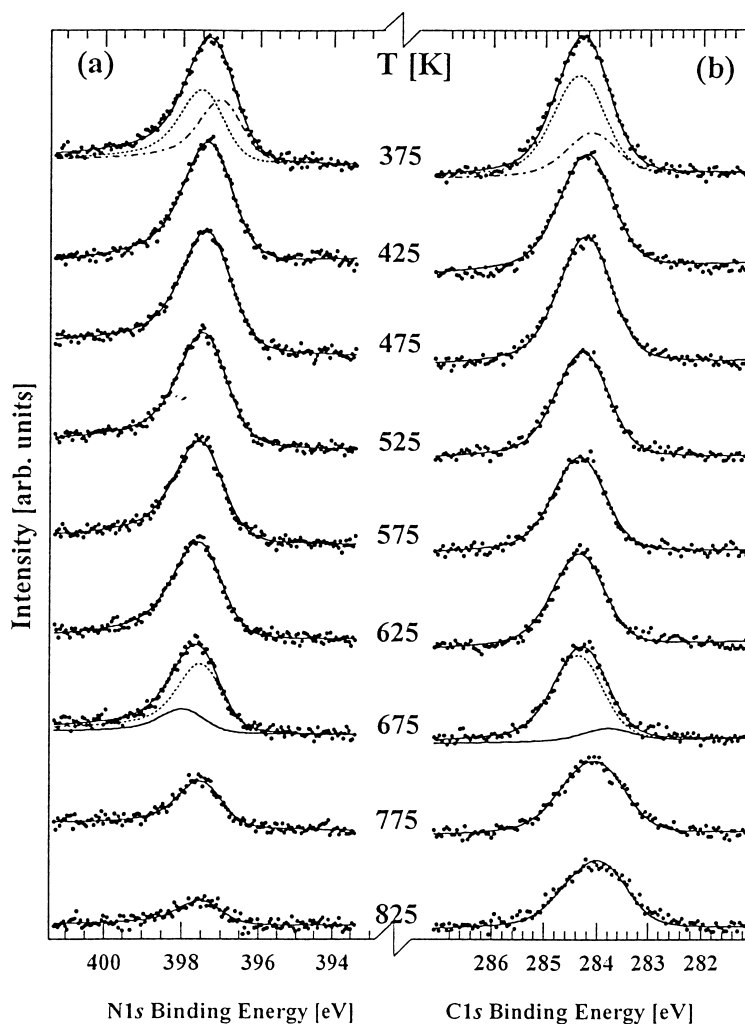


Fig. 6. N 1s (a) and C 1s (b) XPS core-level spectra of the CN saturated Rh(110) surface as a function of annealing the surface to the indicated temperatures.

and C–N bond rupture, which starts at  $\sim 550$ – $600$  K. The  $N_{ad}$  signal first increases to a broad maximum and then decreases again as a result of the recombinative desorption, as indicated by the TDS data. The  $C_{ad}$  remains as a residue at the Rh(110) surface.

#### 4. Discussion

The adsorption of  $C_2N_2$  on Rh(110) above 300 K leads to dissociative adsorption and forma-

tion of CN adlayers. As a function of surface coverage, two CN adsorption states have been identified, which are distinguished by their respective core-level binding energies. It is of interest to compare the two CN surface species on Rh(110) with those found on Pd(110) and Ni(110), for which photoelectron spectroscopy data have also been reported in the literature. On Pd(110), only one CN adsorption state has been detected with C 1s and N 1s binding energies of 284.2 and 397.15 eV, respectively [7]. A previous angle-resolved UV photoemission (ARUPS) study has

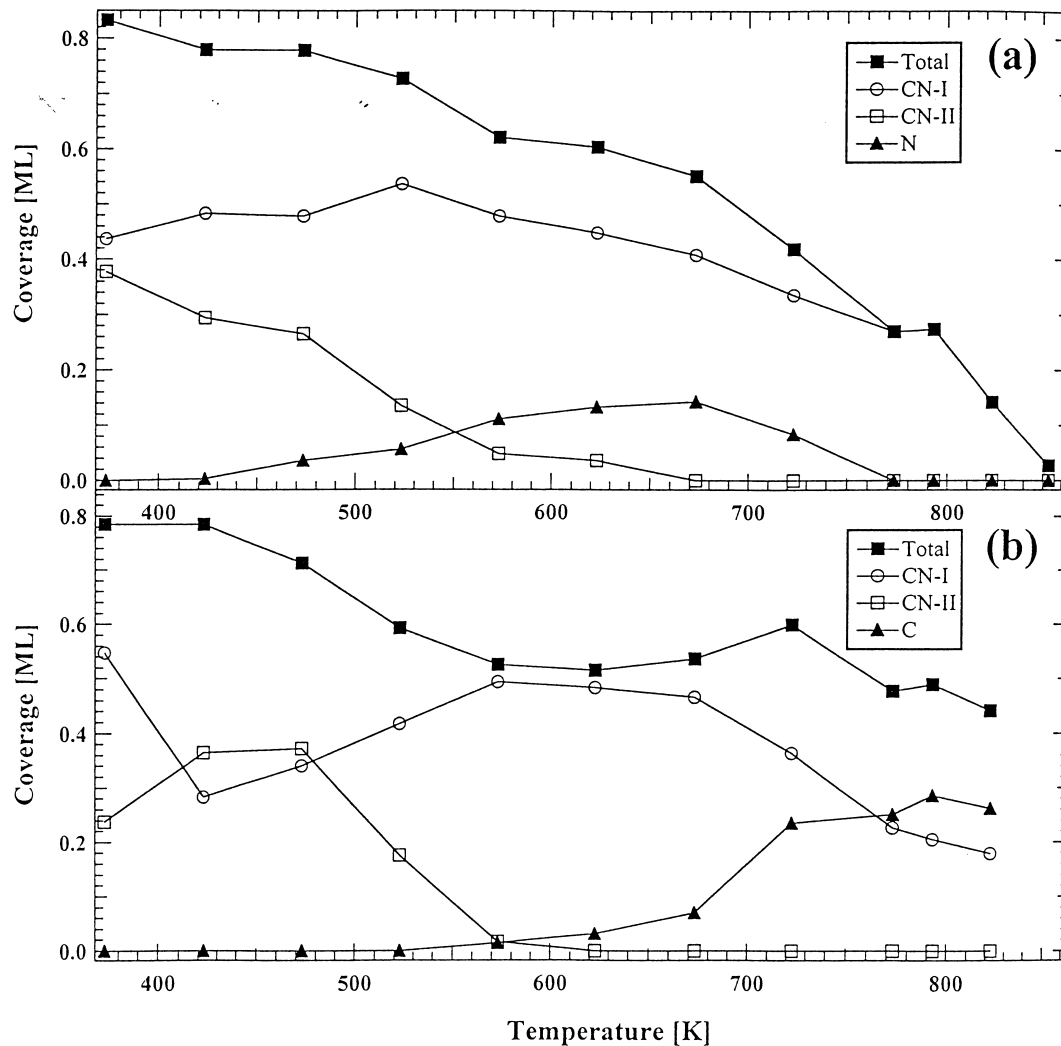


Fig. 7. Plot of the coverages of the various CN derived surface species on Rh(110) as a function of temperature. Panel (a) has been derived from the N 1s XPS spectra of Fig. 6a, panel (b) from the C 1s spectra of Fig. 6b.

placed the CN species on Pd(110) into the grooves of the (110) surface, with an orientation parallel to the  $[1\bar{1}0]$  direction [10]. The situation appears to be more complex on Ni(110). ARUPS and local density functional cluster calculations have indicated that the CN species in the  $c(2 \times 2)$  room-temperature saturation structure on Ni(110) are also flat lying in-groove species, which are oriented parallel to the  $[1\bar{1}0]$  azimuthal direction [11]. However, a recent NEXAFS and photoelectron diffraction (Ph.D.) study of the Ni(110)

$c(2 \times 2)$ -CN surface has concluded that the CN is flat-lying but approximately aligned in the  $[001]$  azimuth [12]. The CN has still been positioned within the grooves of the (110) surface, but in a rather unusual asymmetric site: according to Ph.D. CN lies approximately atop a second-layer Ni atom such that the C atom has similar distances to this second-layer Ni atom and to two top-layer Ni atoms, thus implying essentially a threefold coordination for the C atom. The N atom is then bridge-bonded to two top-layer Ni atoms of the

next close-packed surface atom row [12]. Very recently, XPS and HREELS experiments on the  $c(2 \times 2)$  CN structure on Ni(110) [13,14] have suggested, however, that two CN adspecies might possibly be involved in this adlayer, with the same C 1s BE of 283.3 eV, but with two N 1s BE components of 396.2 and 396.5 eV, implying different environments of the N atoms for the two adsorption states. Additional CN species in a disordered form have been found on Ni(110) that display higher binding energies than the CN species in the  $c(2 \times 2)$  structure and have been associated with various CN-bonding modes in on-ridge configurations [13].

The present results on Rh(110) do not allow a unique specification of the bonding sites of the CN surface species. It is plausible, however, to associate the CN-I state, which is exclusively populated in the  $c(2 \times 2)$  structure, with in-groove CN species, but the orientation and the exact bonding sites must remain uncertain. In view of the close similarity of the C 1s and N 1s binding energies with those of the CN species on Pd(110), we tentatively assign the CN-I state to a flat-lying CN, probably oriented along the  $[1\bar{1}0]$  direction, i.e., parallel to the close-packed Rh rows. The CN-II state, which becomes occupied for higher coverages, beyond the  $c(2 \times 2)$  structure up to the  $c(4 \times 2)$  structure, may then be associated with in-groove species in a tilted configuration, perhaps oriented along  $[001]$ . On-ridge CN species are considered as less likely in view of the higher core-level binding energies observed for these configurations on Ni(110) [13]. In any case, it is likely that various bonding configurations of CN exhibit only small differences in total energy, as recently reported by Yang and Whitten on the basis of total energy calculations of CN on Ni(100) [15]. The two CN configurations as mentioned above will be used in the following to construct the models of the LEED structures, as discussed further below.

The temperature stability of the CN adlayers on Rh(110) is of some interest for the surface chemistry of CN reaction intermediates. For coverages  $<0.5$  ML, CN dissociates completely. The onset of dissociation is around 450 K, as derived from the appearance of the  $C_{ad}$  and  $N_{ad}$  XPS

signals at low CN coverages (not shown). Molecular  $C_2N_2$  desorption is not observed for  $\theta_{CN} < 0.5$ . The  $N_{ad}$  desorbs as  $N_2$  at  $\sim 600$ – $900$  K, whereas  $C_{ad}$  is not removed from the surface by heating. For  $\theta_{CN} > 0.5$  ML, both dissociation and  $C_2N_2$  desorption occur, the latter in a single desorption structure at 540 K at saturation coverage; the shift of the desorption peak from a higher to lower temperature with increasing CN surface coverage is as expected for second-order desorption kinetics. From the XPS results of Fig. 7, it appears that the CN-II state is mostly involved in the desorption process. However, the recombinative desorption of CN at  $\theta_{CN} > 0.5$  is competitive with dissociation, and a redistribution of adsorption states near the desorption temperature may be possible. For the more crowded CN surfaces ( $\theta_{CN} > 0.5$ ), a lower-temperature  $N_2$  desorption peak is observed at 580 K. This desorption state is similar to  $N_2$  from the clean Rh(110) surface [16]. It seems to reflect the desorption of  $N_{ad}$ , which has been generated in the first partial dissociation step of CN in competition with  $C_2N_2$  desorption, in the presence of  $CN_{ad}$  (state I). The  $N_2$  desorption after dissociation of most of the  $CN_{ad}$  at 700–950 K is at a considerably higher temperature than for N adsorption on the clean Rh(110) surface. It is instructive to compare the high-temperature  $N_2$  desorption observed here with the previously published TDS results from a mixed  $C_{ad} + N_{ad}$  layer [17]. The  $N_2$  desorption traces are very similar in these two cases. The high-temperature  $N_2$  desorption has been related to the presence of  $C_{ad}$  at the surface: the diffusion of  $N_{ad}$  is hindered by  $C_{ad}$ , and therefore, the probability of a diffusing N adatom meeting another N atom for recombination and desorption is reduced [17]. However, some reaction-limited desorption of  $N_2$  via CN decomposition cannot be excluded to contribute to the high-temperature desorption structure (see Fig. 7).

The stability of surface CN with temperature appears to be lower on Rh(110) than on Rh(111) surfaces. Solymosi and Bugly [5] and Hwang et al. [6] have reported recombinative  $C_2N_2$  desorption from Rh(111) in several desorption peaks up to more than 800 K, and van Hardevelt et al. [18] have observed that CN groups are stable in the

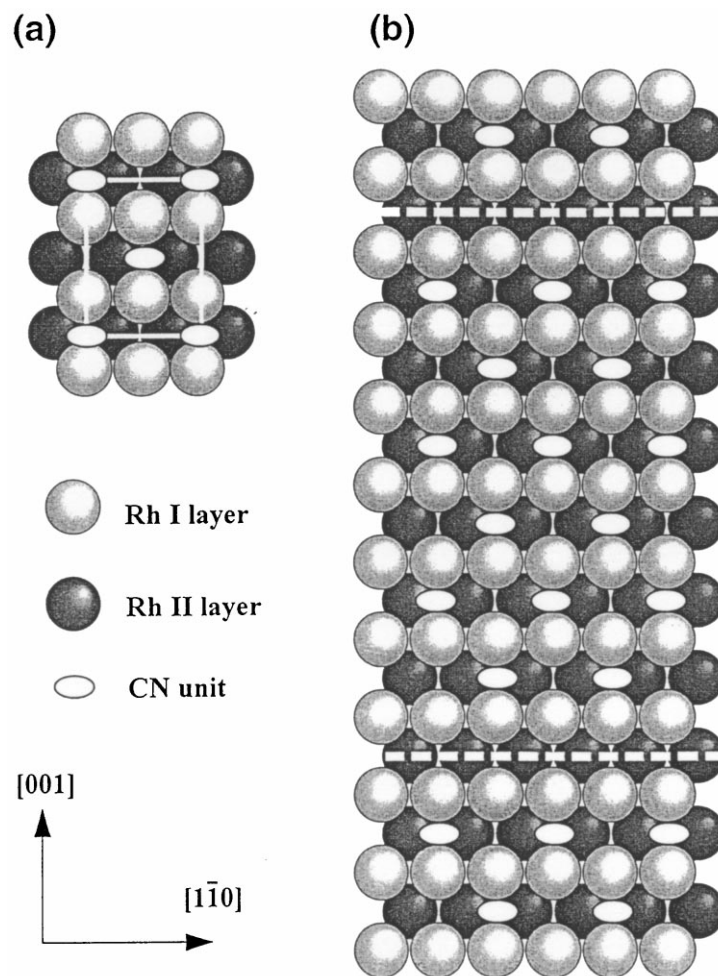


Fig. 8. Schematic models of the  $c(2 \times 2)$ -CN structure (a) and the  $c(2 \times 2)$ -CN structure with reflexes split along the [01] surface direction (b) (the corresponding LEED patterns are shown in Fig. 4b and a, respectively). The dashed lines in (b) indicate the domain boundaries, which are responsible for the splitting of the LEED reflexes.

absence of surface hydrogen up to  $\sim 700$  K. CN decomposition-limited desorption of  $N_2$  on Rh(111) has been detected consistently by all three groups at  $\sim 800$ – $870$  K [5,6,18]. This is considerably higher in temperature than the observed C–N bond breaking temperatures of  $\sim 450$ – $550$  K, depending on coverage, on Rh(110).

Compared with the (110) surfaces of Pd and Ni, the reactivity of Rh(110) for C–N bond rupture is intermediate. Whereas no C–N bond breaking occurs on Pd(110) — all CN can be desorbed as  $C_2N_2$  [7,10] — on Ni(110), some

C–N dissociation occurs already at room temperature [13]. Interestingly, however, Pd(110) has a much greater ability to dissociate  $C_2N_2$  to CN than Rh(110): on Pd(110), the  $C_2N_2$  dissociation reaction is complete at 220 K [7], while on Rh(110), temperatures between 300 and 370 K are required for complete dissociation of  $C_2N_2$  adlayers. Ni(110) again is very reactive, and  $C_2N_2$  undergoes partial dissociation at 90 K [13].

CN on Rh(110) displays two well-ordered LEED structures and interesting transitions between them. Models for these structures will be

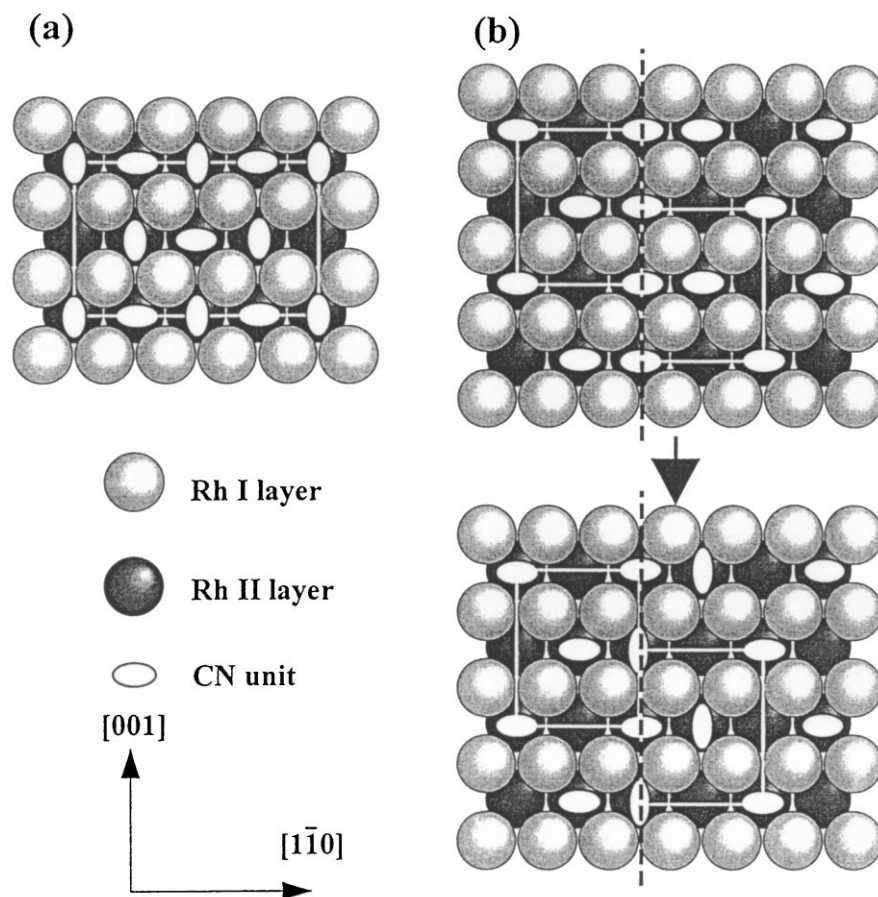


Fig. 9. Schematic models of the  $c(4 \times 2)$ -CN structure (a) and of the  $c(2 \times 2)$ -CN structure with reflexes split along the  $[10]$  surface direction (b) (the corresponding LEED patterns are shown in Fig. 4d and c, respectively). The dashed lines in (b) represent the domain boundaries.

presented in the last part of this discussion. As mentioned above, it is emphasized that the CN adsorption sites adopted for these models are somewhat tentative and arbitrary. However, the general character of the structures and the conclusions drawn on their transitions remain valid, irrespective of the true nature of the CN bonding sites. The  $c(2 \times 2)$  structure of CN on Rh(110) has a domain width of  $\sim 200 \text{ \AA}$ , as judged from the full width at half maximum of the  $(1/2 \ 1/2)$  spots, measured in the SPA-LEED apparatus. This indicates strong long-range interactions between the CN molecules.  $c(2 \times 2)$ -CN structures have also been observed on Pd(110) and Ni(110) surfaces. Fig. 8a shows a schematic model of this

structure, where we have placed the CN in the grooves, parallel to  $[1\bar{1}0]$  in a bridge-bonded site  $[10]$ . The fully developed  $c(2 \times 2)$  structure has been used to calibrate the CN surface coverage with a value of 0.5 ML, but already at  $\sim 0.40 \pm 0.02 \text{ ML}$ , a  $c(2 \times 2)$  structure is observed, albeit with half-order spots split along the  $[01]$  direction (Fig. 4a). The reason for this spot-splitting effect is the existence of domains boundaries and antiphase relationships between them. The splitting direction indicates that the domain walls are oriented along the  $[10]$  direction, i.e., perpendicular to the splitting direction. Careful examination of the separation of the split spots by SPA-LEED gives a separation of  $1/7 a_1$ . This leads to

a model, as shown in Fig. 8b, where the  $c(2 \times 2)$  domains are separated by a domain wall and shifted by one unit cell vector along  $[1\bar{1}0]$  every seventh row. The surface coverage of this model is 0.42 ML, in close agreement with the XPS-derived coverage value. The  $c(2 \times 2)$  domains are separated by so-called light domain walls, which contain no adsorbate species. As the coverage increases from 0.4 to 0.5 ML, the spot splitting decreases due to the growth of  $c(2 \times 2)$  domains, and broad diffuse half-order reflexes develop, as a result of a more random domain size distribution. As the coverage of 0.5 ML is reached, the density of domain walls is low, and the sharp  $c(2 \times 2)$  pattern of Fig. 4b is observed.

The  $c(4 \times 2)$  structure contains two different CN adsorbate configurations, as evidenced by XPS. In our model, they are associated with in-groove species parallel (CN-I) and perpendicular (CN-II) to the  $[1\bar{1}0]$  direction (Fig. 9a). The model shown in the figure yields a coverage of  $7/8$  (0.875) ML, in good agreement with XPS, and is obtained by filling the  $c(2 \times 4)$  structure with CN-I species, four molecules per unit cell, and with CN-II species, three molecules per unit cell. In this way, adsorbate lines are formed with CN species arranged with their axes alternatively parallel and perpendicular to the  $[1\bar{1}0]$  direction.

For coverages between 0.5 and 0.74 ML, LEED patterns with  $(1/2 \ 1/2)$  spot splittings along the  $[10]$  direction have been observed (Fig. 4c). Again, it is suggested that the spot splitting is related to the existence of antiphase domains, with domain boundaries perpendicular to  $[01]$ . The proposed model is a phase between the  $c(2 \times 2)$  and the  $c(4 \times 2)$  structures, with heavy domain walls in this case, i.e., with the local surface coverage being higher than 0.5 in the domain boundaries. The model is presented in Fig. 9b. The idea is that the intermolecular interaction between two adjacent CN species in the domain wall induces a rotation of the molecular axis to reduce repulsion effects, thus creating a precursor arrangement to the  $c(4 \times 2)$  structure. The spot splitting increases with increasing surface coverage until the  $c(4 \times 2)$  structure emerges. In this way, the different models (Figs. 8 and 9) provide a plausible description of the CN surface structures on Rh(110) and of their

transformations, which incorporates consistently both adsorption state and coverage information, as obtained by XPS. A more quantitative description must await LEED intensity analysis, which is presently underway.

## 5. Summary

We have studied the properties of CN adlayers on Rh(110), formed by dissociative adsorption of  $C_2N_2$  at 373 K, as a function of surface coverage and temperature, using LEED, XPS and thermal desorption spectroscopy (TDS). Two different CN adsorption states have been detected by their different C 1s and N 1s XPS binding energies: CN-I is exclusively populated up to 0.5 ML and forms a well-ordered  $c(2 \times 2)$  surface structure. The CN-II species occur additionally at higher CN coverages from 0.5 ML up to the saturation coverage of 0.87 ML, where a  $c(4 \times 2)$  LEED structure is formed. Desorption of CN as molecular  $C_2N_2$  is observed only for coverages  $>0.5$ , and is mainly due to CN-II species. C–N bond rupture is shown to begin at 450–550 K, depending on the CN coverage. The resulting  $N_{ad}$  desorbs at  $\sim 580$  K from the more crowded surfaces and in the range of 650–950 K, whereas  $C_{ad}$  cannot be desorbed thermally. Schematic models for the ordered CN surface structures on Rh(110) and for their transitions are discussed.

## Acknowledgements

We would like to thank Professor Renzo Rosei for helpful discussions. Financial support from the Italian MURST under the program ‘COFIN99’ is acknowledged. F.P.N. acknowledges support from the Austrian Science Foundation.

## References

- [1] R.M. van Hardevelt, A.J.G.W. Schmidt, J.W. Niemantsverdriet, *Catal. Lett.* 41 (1996) 125.
- [2] R.M. van Hardevelt, A.J.G.W. Schmidt, R.A. van Santen,

- J.W. Niemantsverdriet, *J. Vac. Sci. Technol. A* 15 (1997) 1642.
- [3] D.R. Mullins, L. Kundakovic, S.H. Overbury, to be published.
- [4] F.P. Netzer, M.G. Ramsey, *Crit. Rev. Solid State Mater. Sci.* 17 (1992) 397.
- [5] F. Solymosi, L. Bugyi, *Surf. Sci.* 147 (1984) 685.
- [6] S.Y. Hwang, A.C.F. Kong, L.D. Schmidt, *J. Phys. Chem.* 93 (1989) 8327.
- [7] A. Baraldi, S. Lizzit, M.G. Ramsey, F.P. Netzer, *Surf. Sci.* 416 (1998) 214.
- [8] M.G. Ramsey, G. Rosina, F.P. Netzer, H.B. Saalfeld, D.R. Lloyd, *Surf. Sci.* 217 (1989) 140.
- [9] M.G. Ramsey, D. Steinmüller, F.P. Netzer, M. Neuber, L. Ackermann, J. Lauber, N. Rösch, *Surf. Sci.* 260 (1992) 163.
- [10] M.G. Ramsey, G. Rosina, F.P. Netzer, H.B. Saalfeld, D.R. Lloyd, *Surf. Sci.* 218 (1989) 317.
- [11] M.G. Ramsey, D. Steinmüller, F.P. Netzer, S. Köstlmeier, J. Lauber, N. Rösch, *Surf. Sci.* 307–309 (1994) 82.
- [12] N.A. Booth, R. Davis, D.P. Woodruff, D. Chrysostomou, T. McCabe, D.R. Lloyd, O. Schaff, V. Fernandez, S. Bau, K.-M. Schindler, R. Lindsay, J.T. Hoeft, R. Terborg, P. Baumgärtel, A.M. Bradshaw, *Surf. Sci.* 416 (1998) 448.
- [13] R.I.R. Blyth, I. Kardinal, F.P. Netzer, M.G. Ramsey, D. Chrysostomou, D.R. Lloyd, *Surf. Sci.* 415 (1998) 227.
- [14] I. Kardinal, F.P. Netzer, M.G. Ramsey, *Surf. Sci.* 376 (1997) 229.
- [15] H. Yang, J.L. Whitten, *J. Chem. Phys.* 107 (1997) 8518.
- [16] M. Kiskinova, S. Lizzit, G. Comelli, G. Paolucci, R. Rosei, *Appl. Surf. Sci.* 64 (1993) 185.
- [17] S. Lizzit, G. Comelli, Ph. Hofmann, G. Paolucci, M. Kiskinova, R. Rosei, *Surf. Sci.* 276 (1992) 144.
- [18] R.M. van Hardevelt, R.A. van Santen, J.W. Niemantsverdriet, *J. Phys. Chem.* 101 (1997) 7901.